Electronic Supplementary Information (ESI)

Sulfonyldibenzoate Coordination Polymers as Bioactive Dopants for Polysaccharide Films with Antibacterial and Antibiofilm Properties

Tiago A. Fernandes,[ab] Filipa Macedo,[c] Rafaela G. Cabral,[ad] Telma Guiu,[d] Chris H. J. Franco,[a] Paula Jorge,[ce] Ana Catarina Sousa,[ad] Vânia André,[a] Nuno Cerca,*[ce] and Alexander M. Kirillov*[a]

[a] *Centro de Química Estrutural, Institute of Molecular Sciences, Departamento de Engenharia Química, Instituto Superior Técnico, Universidade de Lisboa, Av. Rovisco Pais, 1049-001 Lisbon, Portugal. E-mail: kirillov@tecnico.ulisboa.pt*

[b] *Departamento de Ciências e Tecnologia (DCeT), Universidade Aberta,1000-013 Lisboa, Portugal*

[c] *Centre of Biological Engineering, University of Minho, Campus de Gualtar, 4710-057 Braga, Portugal. E-mail: nunocerca@ceb.uminho.pt*

[d] *Departamento de Engenharia Química, ISEL - Instituto Superior de Engenharia de Lisboa, Instituto Politécnico de Lisboa, R. Conselheiro Emídio Navarro, 1, 1959-007 Lisbon, Portugal*

[e] *LABBELS–Associate Laboratory, Braga/Guimarães, Portugal*

Electronic Supplementary Information (ESI) contains: Materials and Methods; FTIR-ATR spectra (Fig. S1–S4); schematic diagram of $[PS]_n$ and $[PS\text{-}MCC]_n$ biopolymer films (Fig. S5–S6); TGA data (Fig. S6–S9); water absorption data (Table S1); ICP-OES data for silver or copper ions release from biopolymer samples over time (Fig. S10); crystal data and structure refinement details for **1** (Table S2); additional structural details for **1** and **2** (Table S3, Fig. S12); PXRD patterns (Fig. S11); surface analysis (Fig. S13); mechanical properties of films: tensile strength and elongation (Fig. S14); additional antimicrobial data (Fig. S15–S16); crystallographic data in CIF format (CCDC 2245521). See DOI: 10.1039/x0xx00000x

Materials and methods. All chemicals and solvents were purchased from commercial sources. FTIR-ATR spectra were recorded on a Shimadzu IRAffinity-1S apparatus equipped with an ATR ZnSe Performance Crystal Plate accessory. Absorbance spectra were collected in the 4000–400 cm^{-1} range with a 2.0 cm^{-1} resolution using 64 co-added scans (abbreviations: vs − very strong, s − strong, m – medium, w – weak, br – broad, sh − shoulder). EA (elemental analyses) were run on a Perkin Elmer PE 2400 Series II analyzer by Laboratory of Analyses of IST. SEM and SEM-EDX were acquired using a Thermo Scientific, Phenom ProX G6 Desktop SEM, with the accelerating voltage of 25.0 kV. For copper release studies, the determination of Cu content was performed by ICP-OES (Perkin Elmer Optical Emission Spectrometer Optima 2000 DV) with the following operation conditions: RF power 1300 W, auxiliary gas flow 0.2 $L{\cdot}min^{-1}$, nebulizer gas flow 0.6 $L{\cdot}min^{-1}$, plasma flow 15 $L{\cdot}min^{-1}$, Sample Flow Rate 1.50 $mL{\cdot}min^{-1}$, and Cu analytical line 327.393 nm (LAIST, Laboratory of Analyses, IST). Thermogravimetric analyses (TGA) were carried out on a Metler Toledo TGA/DSC-1/1600 HF in the temperature range between 30 and 800 °C and at a heating rate 10 °C/min under oxygen atmosphere. Tensile strength and elongation tests were conducted with an Instron 5966 equipment, using film samples with dimensions of approximately 60 mm × 12 mm × 0.04 mm.

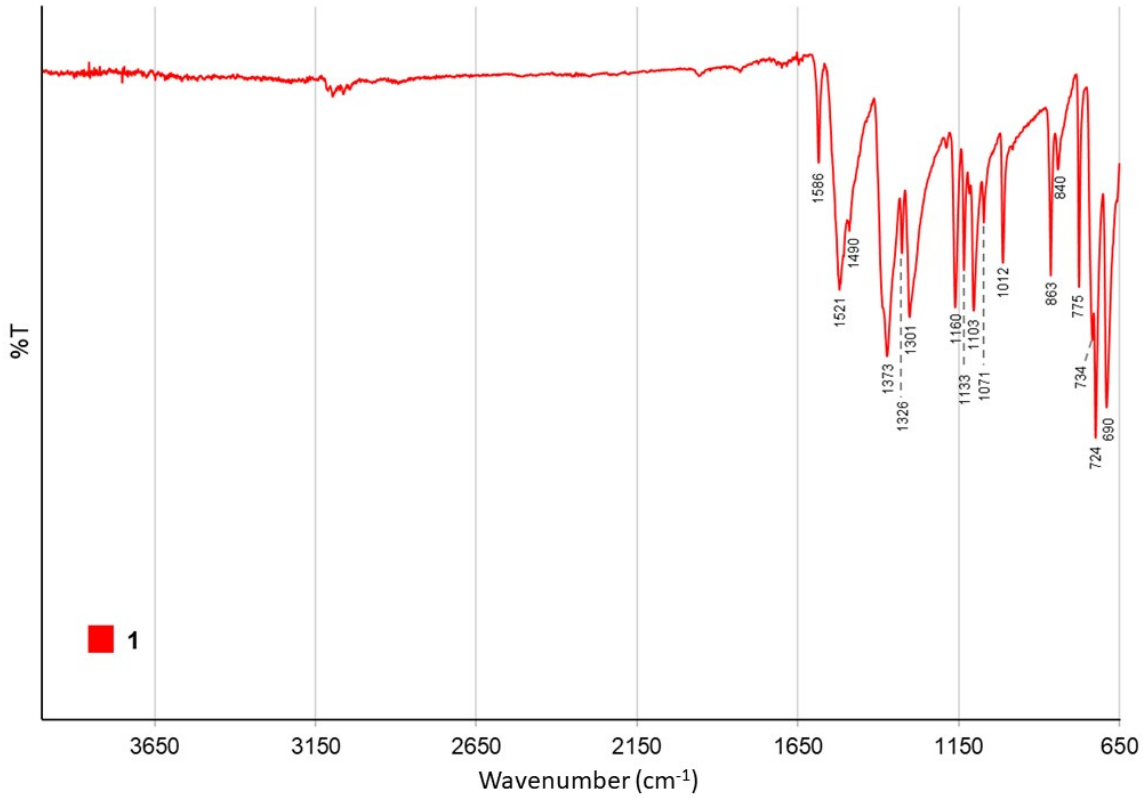

Fig. S1. FTIR-ATR spectrum of **1**.

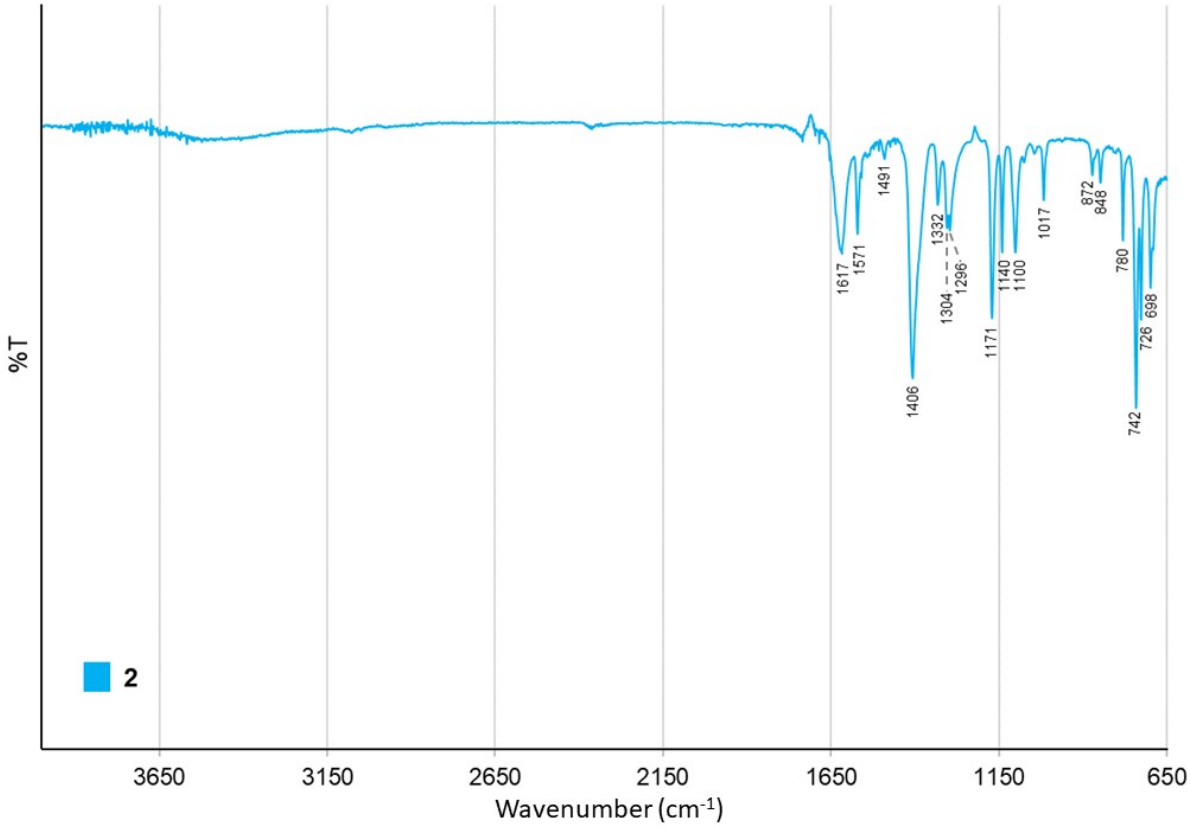

Fig. S2. FTIR-ATR spectrum of **2**.

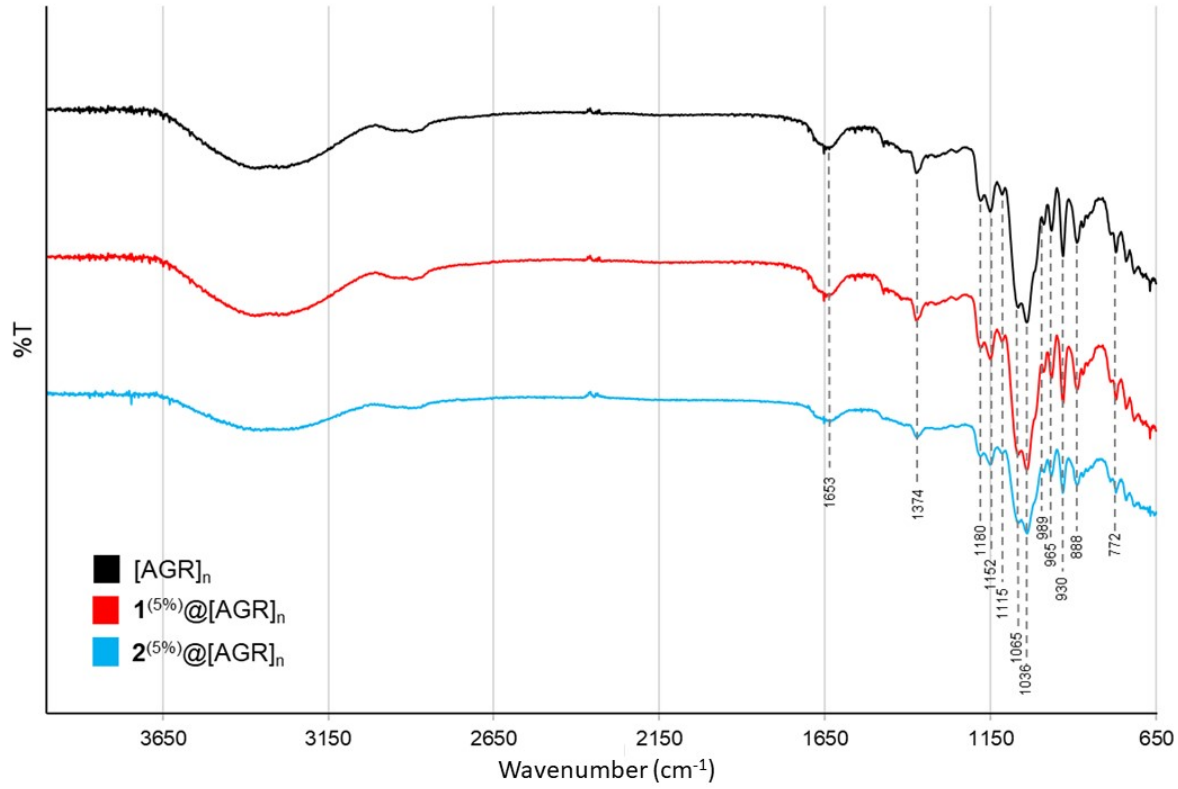

Fig. S3. FTIR-ATR spectra of $[AGR]_n$, $\mathbf{1}^{(5\%)}$@$[AGR]_n$, and $\mathbf{2}^{(5\%)}$@$[AGR]_n$.

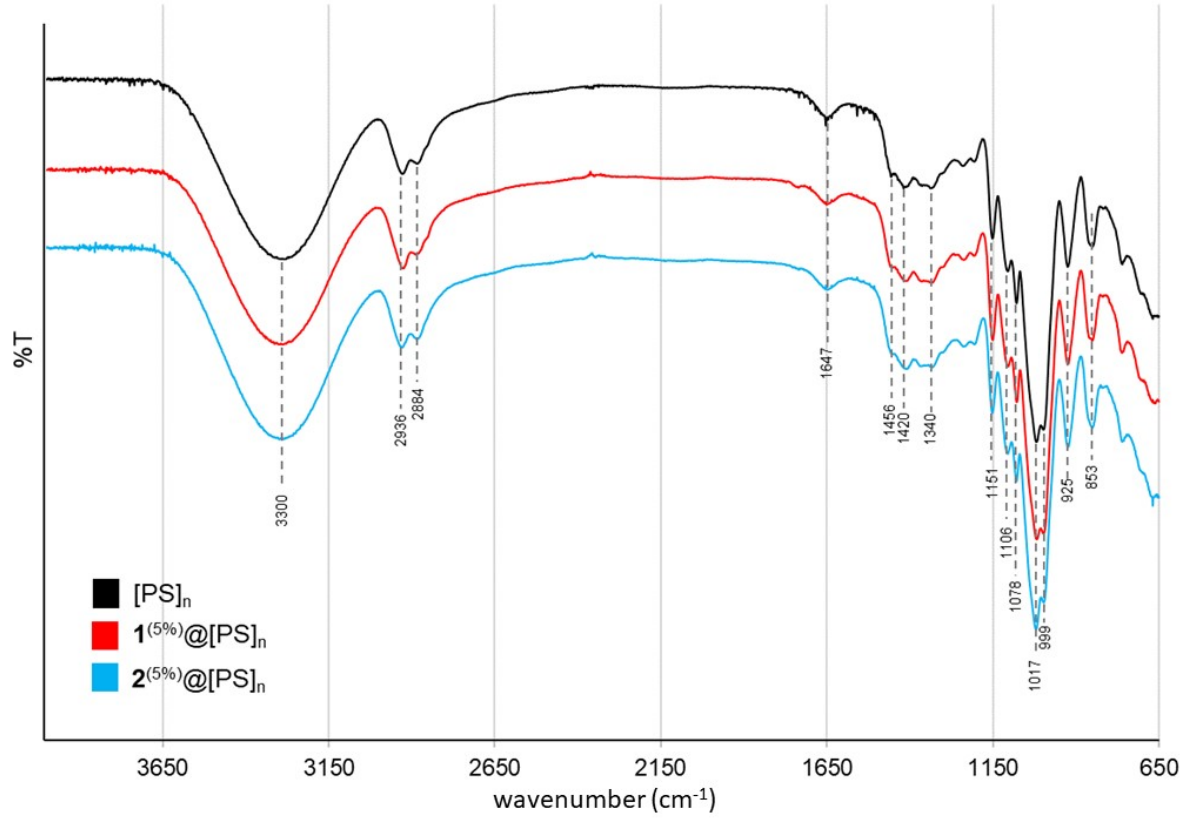

Fig. S4. FTIR-ATR spectra of $[PS]_n$, $\mathbf{1}^{(5\%)}$@$[PS]_n$, and $\mathbf{2}^{(5\%)}$@[$[PS]_n$.

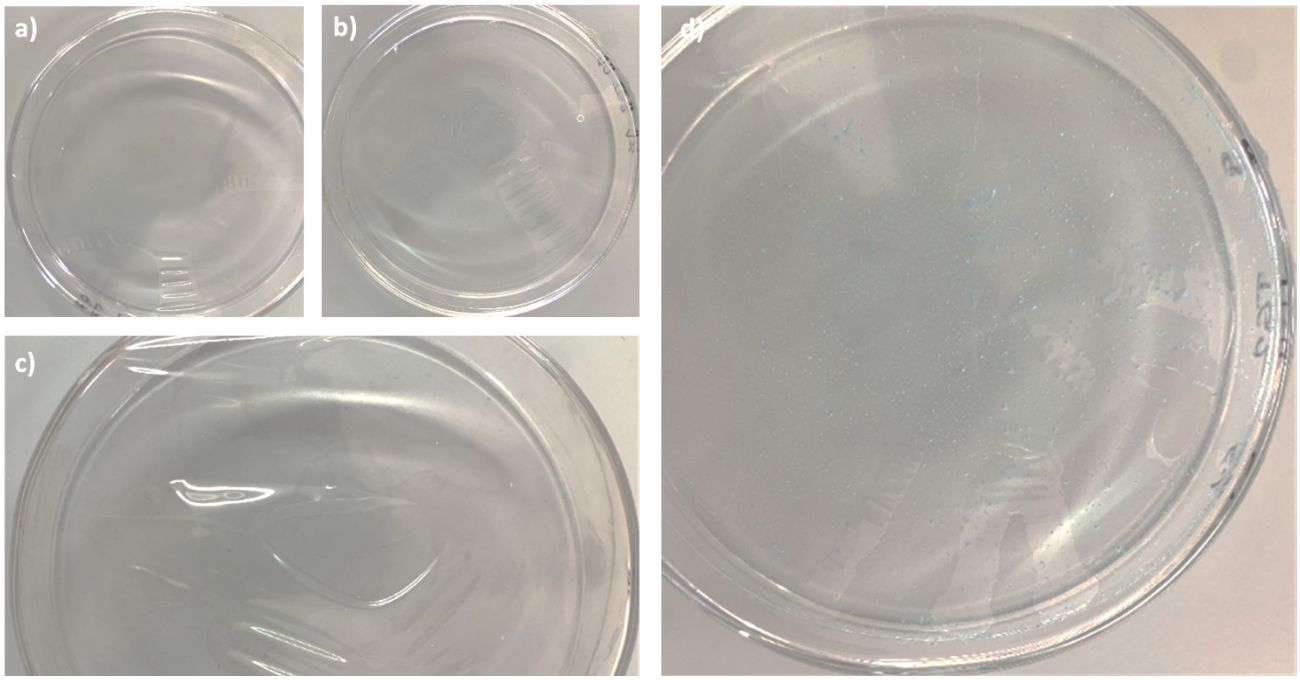

Fig. S5. Biopolymer film photographs for a) **1**$^{(1\%)}$@[AGR]$_n$, b) **2**$^{(1\%)}$@[AGR]$_n$, c) **1**$^{(2.5\%)}$@[AGR]$_n$, and d) **2**$^{(5\%)}$@[AGR]$_n$.

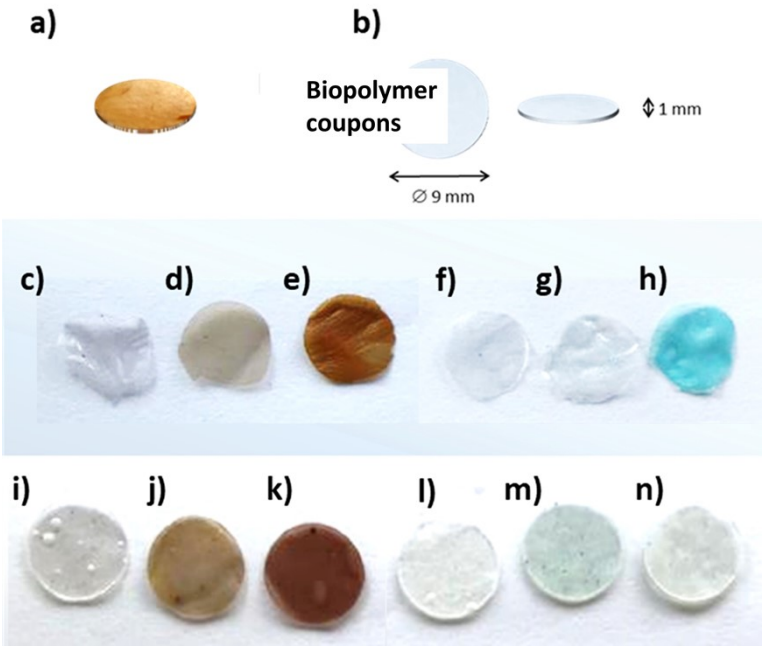

Fig. S6. Sample coupons for a) $[AGR]_n$ and b) $[PS]_n$ translucid biopolymer films. Coupon photographs of c) $\mathbf{1}^{(1\%)}$@$[AGR]_n$, d) $\mathbf{1}^{(2.5\%)}$@$[AGR]_n$, e) $\mathbf{1}^{(5\%)}$@$[AGR]_n$, f) $\mathbf{2}^{(1\%)}$@$[AGR]_n$, g) $\mathbf{2}^{(2.5\%)}$@$[AGR]_n$, h) $\mathbf{2}^{(5\%)}$@$[AGR]_n$, i) $\mathbf{1}^{(1\%)}$@$[PS]_n$, j) $\mathbf{1}^{(2.5\%)}$@$[PS]_n$, h) $\mathbf{1}^{(5\%)}$@$[PS]_n$, l) $\mathbf{2}^{(1\%)}$@$[PS]_n$, m) $\mathbf{2}^{(2.5\%)}$@$[PS]_n$, and n) $\mathbf{2}^{(5\%)}$@$[PS]_n$.

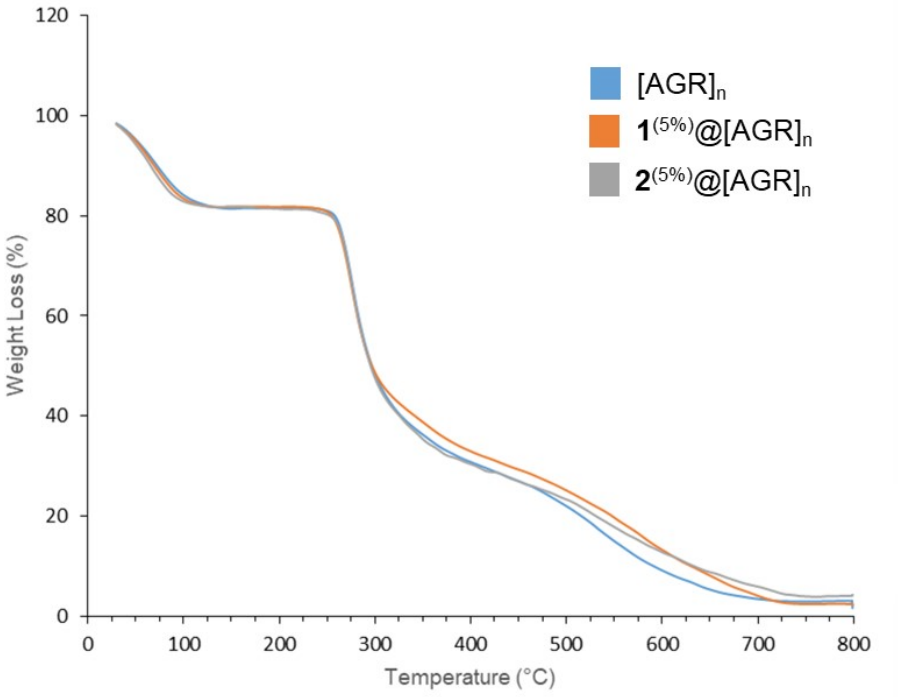

Fig. S7. TGA plots of $[AGR]_n$, $\mathbf{1}^{(5\%)}$@$[AGR]_n$, and $\mathbf{2}^{(5\%)}$@$[AGR]_n$.

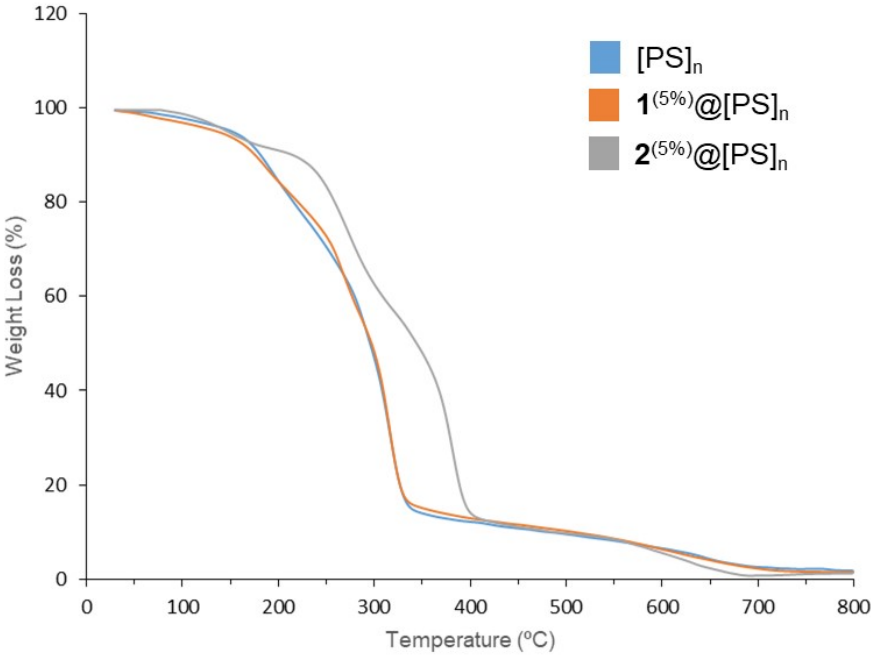

Fig. S8. TGA plots of $[PS]_n$, $\mathbf{1}^{(5\%)}@[PS]_n$, and $\mathbf{2}^{(5\%)}@[PS]_n$.

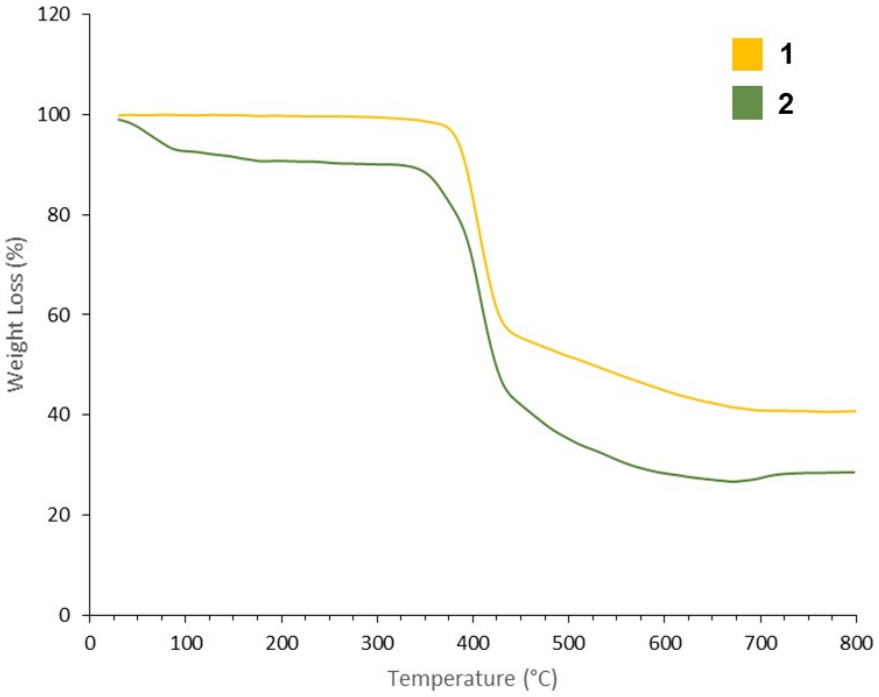

Fig. S9. TGA plots of **1** and **2**.

Water absorption by biopolymers. In order to investigate water absorption by the obtained samples, the biopolymer films (~50 mg) were submerged in water (20 mL; 36 °C) and their mass was determined after 24 and 48 h (Table S1). The % of water absorption was calculated by the following equation:

$$W_{up}\,(\%) = \frac{W_f - W_i}{W_i} \times 100$$

Table S1. Water absorption determination through mass weighing for $[AGR]_n$ biopolymer films.

Biopolymer	Sample	W_i (mg)[a]	W_f (mg)[b]		W_{up} (%)[c]		Average W_{up} (%)
		0 h	24 h	48 h	24 h	48 h	24 h (48h)
$[AGR]_n$	a	9.3	29.1	28.3	212.9	204.3	214.6 (213.8)
	b	9.9	31.3	32.0	216.2	223.2	
$[PS]_n$	a	16.7	21	21.2	25.8	26.9	26.9 (29.3)
	b	18.9	24.2	24.9	28.0	31.7	

[a]Starting weight. [b]Weight after 24 and 48 h. [c]Water uptake weight percentage after 24 and 48 h.

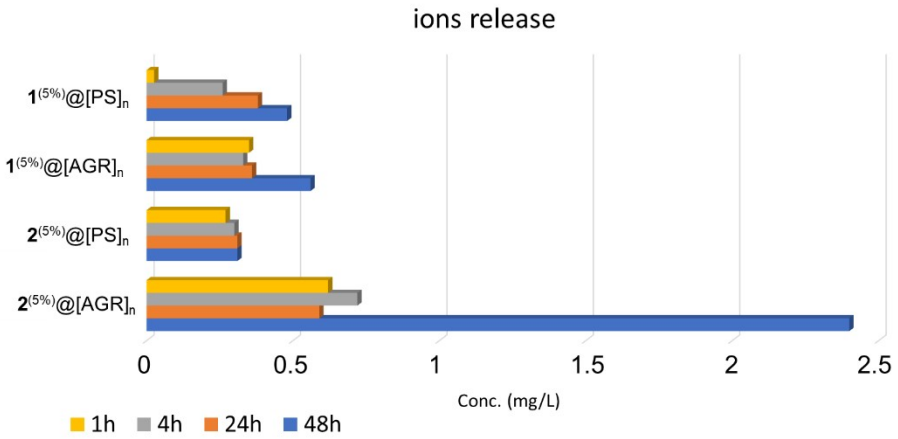

Fig. S10. ICP-OES data for silver or copper ion release from **1**@$[AGR]_n$, **2**@$[AGR]_n$, **1**@$[PS]_n$, and **2**@$[PS]_n$ with doping percentages of 5% (m/m) after 1, 4, 24, and 48 h in aqueous PBS solution.

For the $[AGR]_n$ film doped by 5% of **1**, during the first 24 h, there was an average metal ion release of 0.35 mg/L with a standard deviation of 0.014. After 48 h, a considerable increase in the release of silver ions was observed (0.56 mg/L). During the first 24 h, the trend for **2**$^{(5\%)}$@$[AGR]_n$ was maintained with a release of the same order of magnitude, with an average value of 0.643 mg/L for the released copper ions, with a standard deviation of 0.0556. After 48 h, there was a significant increase in the release of copper ions (2.4 mg/L).

Ag release of 0.56 mg/L corresponds to ~1.1% of all silver present in $\mathbf{1}^{(5\%)}$@$[AGR]_n$ and Cu release of 2.4 mg/L corresponds to ~12.1% of all copper present in $\mathbf{2}^{(5\%)}$@$[AGR]_n$.

Structural details for compounds 1 and 2

Table S2. Crystal data and structure refinement details for **1**.

	1
Formula	$C_{14}H_8Ag_2O_6S$
Fw	520.00
Crystal form, colour	Prism
Crystal size (mm)	0.16 × 0.08 × 0.04
Crystal system	Monoclinic
Space group	$P2_1/m$
a, *b*, *c*, Å	5.2438 (3), 24.1388 (15), 5.7764 (4)
β, °	114.179 (2)
Z	2
V, Å^3	667.03 (7)
D_c, g cm^{-3}	2.589
μ(MoKα)	0.71073
μ, mm^{-1}	3.122
$(\sin\theta/\lambda)_{max}$ (Å^{-1})	0.602
refl. collected	19333
independent refl.	1237
R_{int}	0.036
R_1 [a], wR_2 [b] [$I \geq 2\sigma(I)$]	0.062, 0.125
GOF on F^2	1.18
Crystallization solvent	Acetonitrile/methanol/Water mixture

[a] $R_1 = \Sigma||F_o| - |F_c||/\Sigma|F_o|$. [b] $wR_2 = [\Sigma[w(F_o^2 - F_c^2)^2]/\Sigma[w(F_o^2)^2]]^{1/2}$

Table S3. Selected geometric parameters for compound **1** (Å, °).

Distances (Å)			
Ag1—Ag1^{i}	2.8521 (17)	Ag1—O1^{i}	2.171 (5)
Ag1—O2	2.152 (5)		
Angles (°)			
O2—Ag1—O1^{i}	163.5 (2)	C5^{ii}—S1—C5	102.3 (4)
O1^{iii}—Ag1—Ag1^{i}	151.06 (12)		

Symmetry codes: (i) −x−1, −y+1, −z+1; (ii) x, −y+1/2, z; (iii) x, y, 1+z.

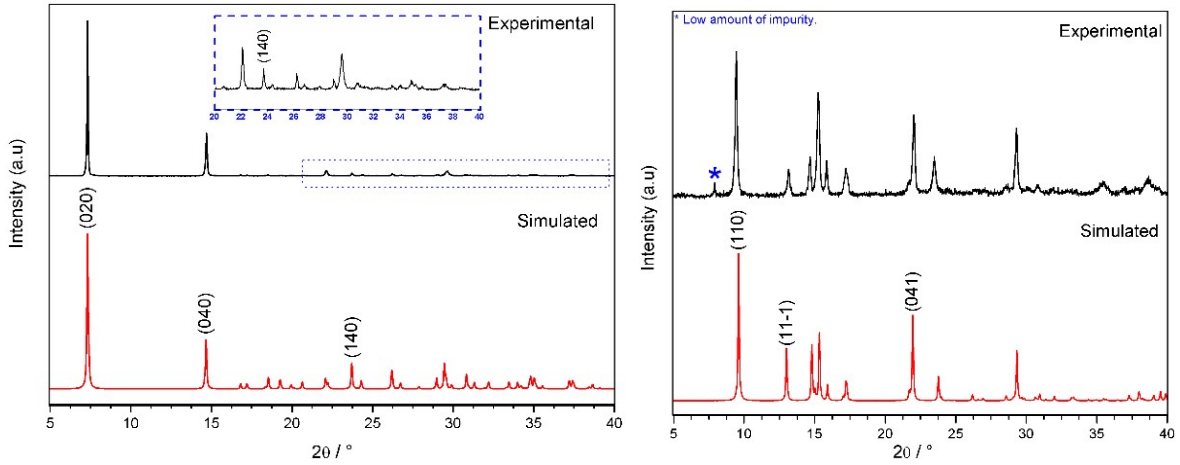

a) b)

Fig. S11. PXRD patterns of a) $[Ag_2(H_2\text{-sdba})]_n$ (**1**) and b) $\{[Cu(sdba)\cdot H_2O]\cdot 1.5H_2O\}_n$ (**2**).

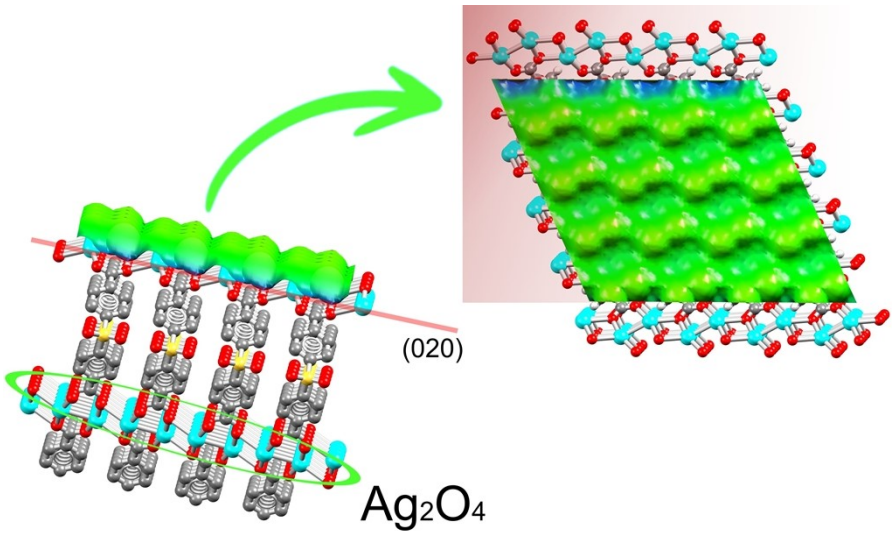

Fig. S12. Representation of the (020) crystal face for compound **1**. Ag_2O_4 units are more exposed in this face.

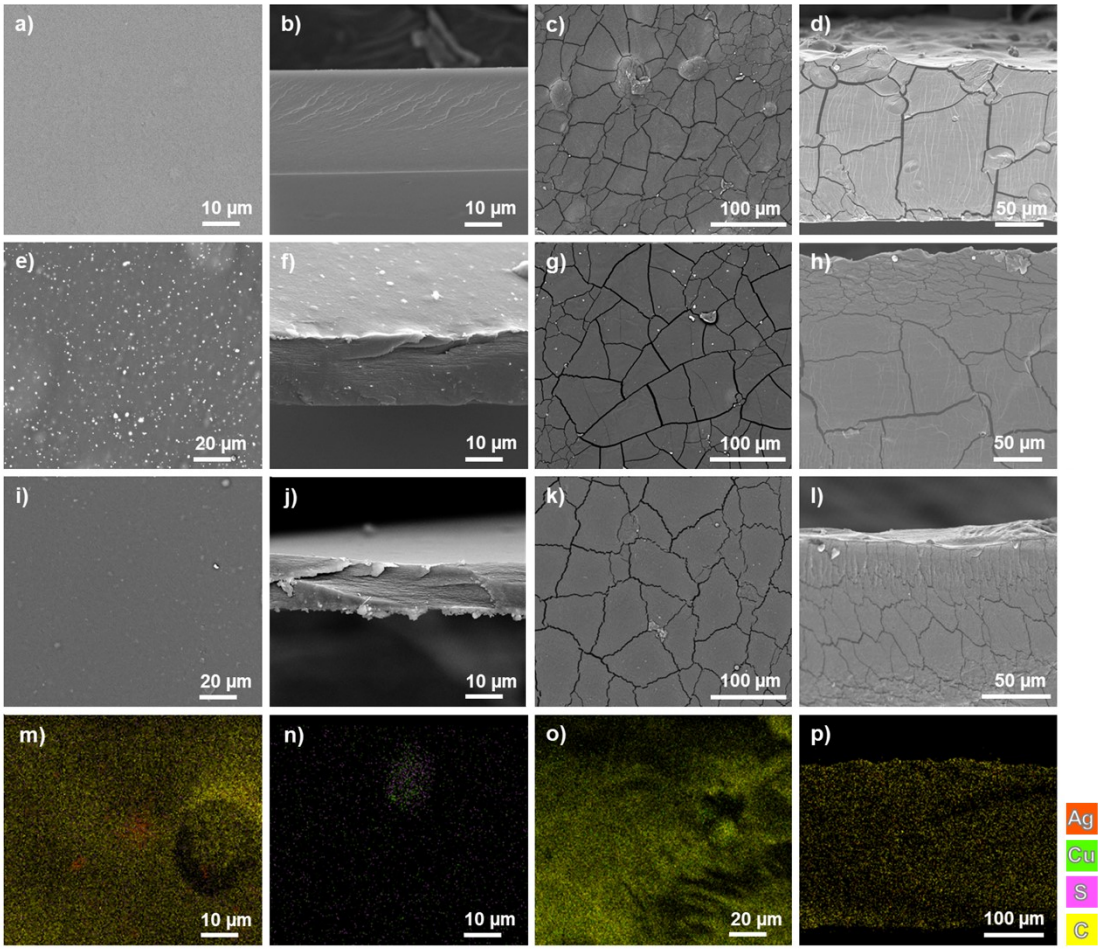

Fig. S13. Morphology characterization using SEM-EDX. SEM images of a) $[AGR]_n$; b) $[AGR]_n$ cross section; c) $[PS]_n$; d) $[PS]_n$ cross section; e) $\mathbf{1}^{(5\%)}$@$[AGR]_n$; f) $\mathbf{1}^{(5\%)}$@$[AGR]_n$ cross section; g) $\mathbf{1}^{(5\%)}$@$[PS]_n$; h) $\mathbf{1}^{(5\%)}$@$[PS]_n$ cross section; i) $\mathbf{2}^{(5\%)}$@$[AGR]_n$; j) $\mathbf{2}^{(5\%)}$@$[AGR]_n$ cross section; k) $\mathbf{2}^{(5\%)}$@$[PS]_n$; l) $\mathbf{2}^{(5\%)}$@$[PS]_n$ cross section; m) $\mathbf{1}^{(5\%)}$@$[AGR]_n$, with an EDX analysis of Ag, C, and S distribution; n) $\mathbf{2}^{(5\%)}$@$[AGR]_n$, with an EDX analysis of Cu and S distribution; o) $\mathbf{2}^{(5\%)}$@$[PS]_n$, with an EDX analysis of Cu and C distribution; p) $\mathbf{2}^{(5\%)}$@$[PS]_n$ cross-section top-down, with an EDX analysis of Ag and C distribution; m) 2000× magnification; a), b), f), and j) 1200× magnification; n) 1000× magnification; e) and o) 500× magnification; l) 270× magnification; c), g), i), and k) 200× magnification; d), h), and p) 160× magnification.

The bioCP-doped $[AGR]_n$ and $[PS]_n$ biopolymer films were examined by SEM–EDX (Fig. S13) to further evaluate their morphology and incorporation of **1** or **2** into the films. The analyses were carried using the samples dried in the desiccator for one week. The two films, $[AGR]_n$ and $[PS]_n$, have highly distinct morphologies, as seen in Fig. 5a-d. The surface of the $[AGR]_n$ films is smoother and uniform when compared to that of $[PS]_n$. The $[PS]_n$ matrices showed a sludgy surface with inhomogeneous granules (Fig. S13c). Figs. 5e,g represent the surfaces of the two different matrices doped by compound **1**, while Figs. 5f,h show their cross sections. The dopants contribute to significantly different morphologies on the surface of $[AGR]_n$ films, featuring bioCPs agglomerates across the material's surface (Figs. S13e,i). On the other hand,

differences in the surfaces of doped $[PS]_n$ films were blurred (Fig. S13g,k). Both materials were then evaluated by SEM–EDX using silver or copper probes for determining the distribution of Ag or Cu (Figs. S13m-p). Ag and Cu mapping images of the $\mathbf{1}^{(5\%)}$@$[AGR]_n$ and $\mathbf{2}^{(5\%)}$@$[AGR]_n$ films (Fig. S12m,n) show that silver or copper were barely present on the surface of coupons, as was found for all the doped films and on both sides. The surface was primarily composed of carbon and oxygen, with just a few accumulations of silver or copper. When these accumulations emerged, they were accompanied with sulfur agglomerations present in the sulfonyldibenzoate ligands (Fig. S13m,n). The same was observed for $\mathbf{2}^{(5\%)}$@$[PS]_n$. By splitting the coupons, it was possible to analyze the cross-sections. Within a 1 mm thick film of $\mathbf{1}^{(5\%)}$@$[PS]_n$, there is eventually a uniform dispersion of silver with occasionally increased concentrations in sections containing larger crystalline particles of **1**. The other doped films followed the same trend. When examining the full sample coupon, any potential variation in the distribution of Ag or Cu was minimal, as indicated by good repeatability of biological assays performed in triplicate for doped films.

Mechanical properties

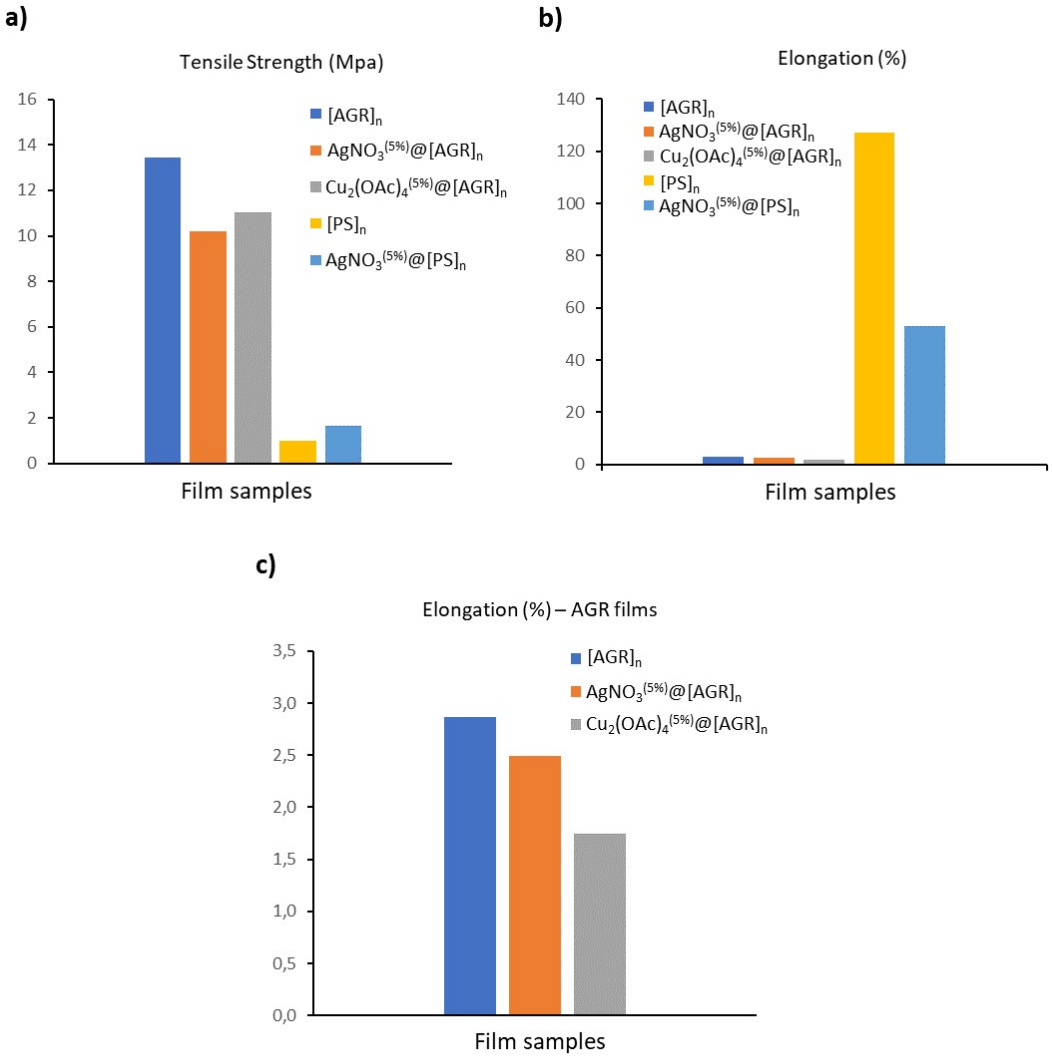

Fig. S14. Mechanical properties of films: a) tensile strength (MPa); b) elongation (%); c) zoom of elongation for agarose films.

Antibacterial activity controls

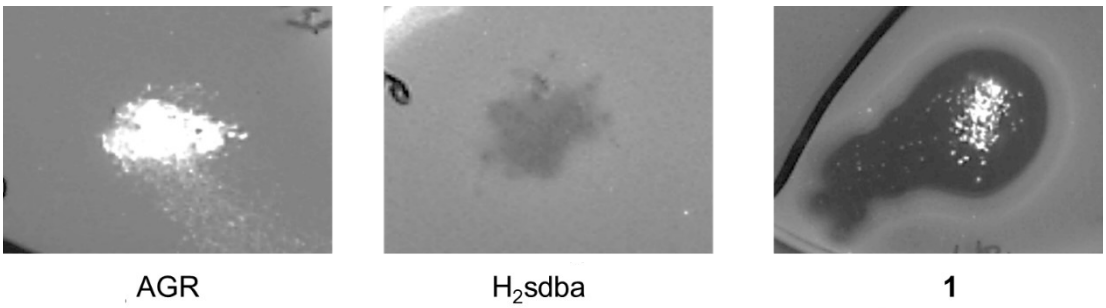

Fig. S15. Antibacterial activity of the two controls AGR and H_2sdba and of the bioCP **1** against *Staphylococcus epidermidis* RP62A.

The base powder formulation of the $[AGR]_n$ matrix and of the ligand H_2sdba did not show any antibacterial activity, as seen by the lack of growth inhibition halo around them. In contrast, a substantial growth inhibition halo can be seen for bioCP **1**.

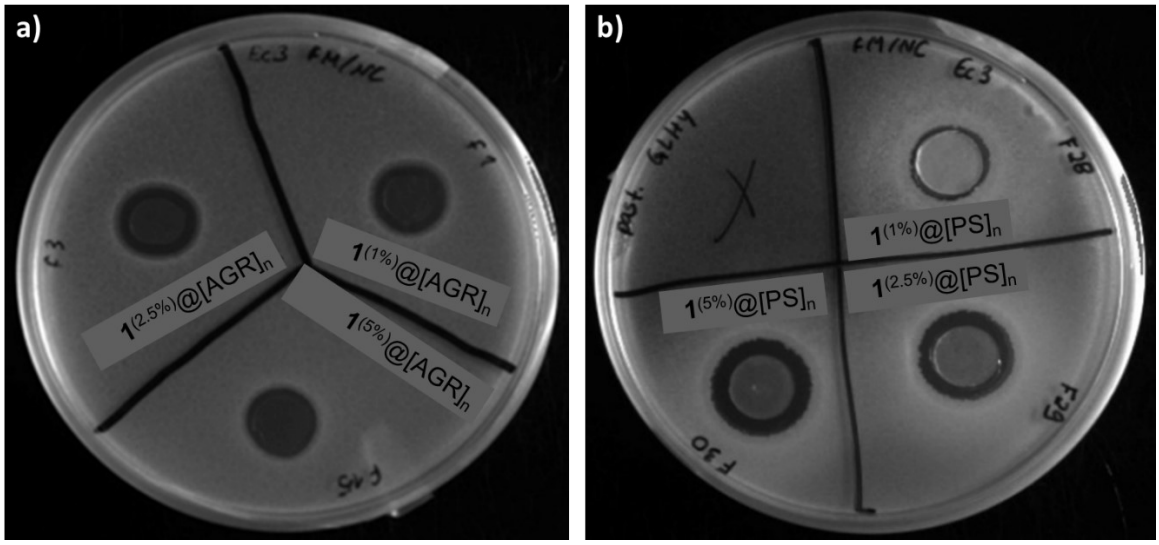

Fig. S16. Representative antibacterial activity photographs for *Escherichia coli* inhibition assays for a) **1**@$[AGR]_n$ and b) **1**@$[PS]_n$.

Supplementary references

1 P.M. Shafi and A.C. Bose, Impact of crystalline defects and size on X-ray line broadening: A phenomenological approach for tetragonal SnO_2 nanocrystals. *AIP Advances.*, 2015, **5**, 057137.

2 V. Biju, N. Sugathan, V. Vrinda and S.L. Salini, Estimation of lattice strain in nanocrystalline silver from X-ray diffraction line broadening. *J Mater Sci*., 2008, **43**, 1175.